ISSN 1674-1056
http://cpb.iphy.ac.cn
http://iopscience.iop.org/cpb
中国物理 B
Chinese Physics
中国物理
Chinese Physics B

Magnetic properties of the double perovskite compound Sr_2YRuO_6

N. EL Mekkaoui, S. Idrissi, S. Mtougui, I. EL Housni, R. Khalladi, S. Ziti, H. Labrim, L. Bahmad
Citation: Chin. Phys. B . 2019, 28(9): 097503 . **doi:** 10.1088/1674-1056/28/097503
Journal homepage: http://cpb.iphy.ac.cn; http://iopscience.iop.org/cpb

What follows is a list of articles you may be interested in

Computational study of inverse ferrite spinels

A EL Maazouzi, R Masrour, A Jabar, M Hamedoun
Chin. Phys. B . 2019, 28(5): 057504 . **doi:** 10.1088/1674-1056/28/5/057504

Phase diagrams and magnetic properties of the mixed spin-1 and spin-3/2 Ising ferromagnetic thin film:Monte Carlo treatment

B Boughazi, M Boughrara, M Kerouad
Chin. Phys. B . 2019, 28(2): 027501 . **doi:** 10.1088/1674-1056/28/2/027501

Effect of particle size distribution on magnetic behavior of nanoparticles with uniaxial anisotropy

S Rizwan Ali, Farah Naz, Humaira Akber, M Naeem, S Imran Ali, S Abdul Basit, M Sarim, Sadaf Qaseem
Chin. Phys. B . 2018, 27(9): 097503 . **doi:** 10.1088/1674-1056/27/9/097503

Typicality at quantum-critical points

Lu Liu(刘录), Anders W Sandvik, Wenan Guo(郭文安)
Chin. Phys. B . 2018, 27(8): 087501 . **doi:** 10.1088/1674-1056/27/8/087501

Asymmetric response of magnetic impurity in Bernal-stacked bilayer honeycomb lattice

Jin-Hua Sun(孙金华), Ho-Kin Tang(邓皓键)
Chin. Phys. B . 2018, 27(7): 077502 . **doi:** 10.1088/1674-1056/27/7/077502

Magnetic properties of the double perovskite compound Sr_2YRuO_6

N. EL Mekkaoui[1,†], S. Idrissi[1], S. Mtougui[1], I. EL Housni[1], R. Khalladi[1], S. Ziti[2], H. Labrim[3], and L. Bahmad[1,‡]

[1] *Laboratoire de la Matière Condensée et des Sciences Interdisciplinaires (LaMCScI), Mohammed V University, Faculty of Sciences, B.P.* 1014 *Rabat, Morocco*
[2] *Intelligent Processing and Security of Systems, Mohammed V University in Rabat, Faculty of Sciences, B.P.* 1014 *Rabat, Morocco*
[3] *USM/DERS/ Centre National de l'Energie, des Sciences et des Techniques Nucléaires (CNESTEN), Rabat, Morocco*

(Received 15 February 2019; revised manuscript received 10 July 2019; published online 30 August 2019)

We study the magnetic properties of the double perovskite ruthenate compound Sr_2YRuO_6 using Monte Carlo simulations (MCS). We elaborate the ground state phase diagrams for all possible and stable configurations. The magnetizations and the susceptibilities as a function of temperature for the studied system are also reported. The effects of the exchange coupling interactions and the crystal field are examined and discussed. On the other hand, since the compound Sr_2YRuO_6 exhibits an antiferromagnetic behavior, we find its Néel temperature, $T_N \approx 31$ K, which is in good agreement with the experimental results in the literature. To complete this study, the hysteresis loops and the coercive field as a function of the external magnetic field are also obtained for fixed values of the physical parameters.

Keywords: Monte Carlo, Ising model, antiferromagnetics, magnetic properties of nanostructures

PACS: 75.75.–c, 05.10.Ln, 64.60.De, 75.50.Ee **DOI:** 10.1088/1674-1056/ab3441

1. Introduction

The compound Sr_2YRuO_6 belongs to the family of double perovskites with general formula $A_2BB'O_6$, where the site occupied by a large cation A = Ca, Sr, Ba is capable of 12-fold coordination by oxygen, while the B and B' sites represent smaller cations suitable for octahedral coordination, generally being lanthanides, yttrium, or 4d/5d transition metals.[1,2] The compound Sr_2YRuO_6 is really interesting, with a frail equilibrium between ferromagnetic (FM) and antiferromagnetic (AFM) interactions engendering a complex magnetic response initially described as "anomalous".[1] The compound Sr_2YRuO_6 crystallizes in the ordered double perovskite structure with Ru^{5+} ions described by an FCC magnetic system, which align in an AFM structure at low temperature.[3] Specific heat and magnetic susceptibility measurements reveal two phase transitions at $\sim$ 30 K and $\sim$ 26 K respectively,[1] while the physical state of Sr_2YRuO_6 between these two transition temperatures continues to be elucidated. Additional interest in this material is originated from the occurrence of superconductivity when Ru is partially (up to 15%) replaced by Cu in both powders[3–7] and single crystals,[8–10] with superconducting volume fractions still under 10%. A broad knowledge of the magnetic state of Sr_2YRuO_6 is fundamental to understand how the superconducting and ferromagnetic order parameters can adjust themselves in the crystal lattice.[11] However, since only one magnetic sublattice is present in Sr_2YRuO_6, this knowledge will contribute to the characterization of other double perovskites with two magnetic sublattices, like Sr_2FeReO_6 and Sr_2FeMoO_6 which are interesting for their potential application in spin electronics at room temperature.[12] Hence, even though Sr_2YRuO_6 was synthesized 30 years ago as reported in Ref. [13], crucial and precise analysis of the experimental results with different techniques is still needed. The anomalies possess unusual transport and magnetic properties that emphasize the strong interplay of spin, charge, and orbital degrees of freedom. In some of our recent works,[14–23] we have provided the magnetic behavior and phase diagrams using Monte Carlo simulations for the perovskite $BiFeO_3$, also we have presented and discussed the corresponding hysteresis cycles.

Within this context, the goal of this paper is to make a theoretical investigation of the magnetic properties of the Sr_2YRuO_6 compound. To reach this goal, a thoughtful analysis of the ground states, magnetizations, and susceptibilities as a function of the temperature and the effect of the crystal field along with the behavior of the hysteresis loop are discussed.

This paper is organized as follow. In Section 2, we present the model and the Hamiltonian describing the compound Sr_2YRuO_6. Section 3 is devoted to the interpretation of the obtained results from the ground state phase diagrams as well as from the Monte Carlo simulations. In Section 4, we provide our conclusions.

2. Theoretical model

The theoretical model used to simulate the magnetic properties of the double perovskite Sr_2YRuO_6 using Monte Carlo simulation is presented in this section. The structure of the studied compound corresponds to the space group P_{21}/n as presented in Fig. 1.[24] The unit cell crystal structure of Sr_2YRuO_6 is illustrated in Fig. 1(a), whereas the octahedrons

†Corresponding author. E-mail: n.elmekkaoui@gmail.com
‡Corresponding author. E-mail: bahmad@fsr.ac.ma

© 2019 Chinese Physical Society and IOP Publishing Ltd

of RuO_6 and YO_6 are presented in Fig. 1(b). The structural parameters of Sr_2YRuO_6 are listed in Table 1 according to Ref. [25]. The coordinates of the atoms Sr, Y, Ru, O1, O2, and O3 are given in Table 2.[25]

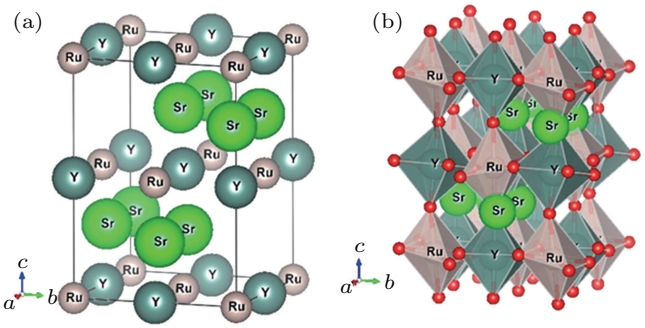


Fig. 1. (a) The unit cell crystal structure of Sr_2YRuO_6, and (b) RuO_6, YO_6 octahedrons.

Table 1. Structure parameters of Sr_2YRuO_6.[25]

Structure parameters	Values
Space group	$P21/n$
Cell parameters	$a = 5.7761$ Å, $b = 5.7840$ Å, $c = 8.1689$ Å, $\alpha = \gamma = 90°$, $\beta = 90.2087°$

Table 2. Coordinates of Sr_2YRuO_6.[25]

Site	X	Y	Z	Magnetic moment/μ_B
Sr	0.0053	0.0267	0.2379	0
Y	1/2	0	0	0
Ru	1/2	0	1/2	3/2
O1	0.2648	0.2954	0.0338	0
O2	0.1988	0.7710	0.0345	0
O3	0.9331	0.4865	0.2352	0

The magnetic ordering of this compound can occur only by the Ru moments as illustrated in Fig. 2. The Hamiltonian controlling the system reads

$$H_S = -J_{\parallel} \sum_{\langle i,j \rangle} S_i^{\parallel} S_j^{\parallel} - J_{\perp} \sum_{\langle i,j \rangle} S_i^{\perp} S_j^{\perp} - H \sum_i S_i - \Delta \sum_i S_i^2. \quad (1)$$

In the above equation, the notation $\langle i, j \rangle$ corresponds to the nearest-neighbors' spins. The spins S_i of the Ru atom take the values $\pm 1/2$, $\pm 3/2$. The exchange coupling constant is donated by J. The last two terms are the Zeeman energy and the crystal field energy, where H and Δ are the external magnetic field and the crystal field, respectively. The notations $\perp$ and $\parallel$ stand for the perpendicular and parallel directions. The external magnetic field H and the crystal field Δ are acting on all the system spins. The crystal field is originated from the competition between Ru–O interactions in this compound. In order to simulate this system's magnetic behavior, with the above Hamiltonian, Monte Carlo simulations are performed under the Metropolis algorithm.

In this work, we give all physical parameters in the MKSA units. In fact, the temperature is in Kelvin, the energies are in Joule, and the external magnetic and crystal fields are in Tesla. For simplicity, we have fixed the Boltzmann constant at its unit value $K_B = 1$ (dimensionless). This is the case for the earlier references.[15,16,20,23,26–28]

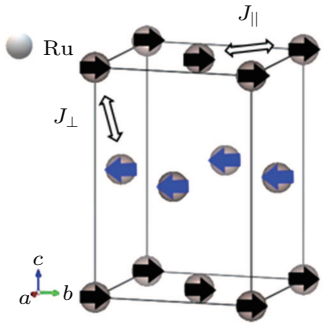


Fig. 2. The unit cell of Sr_2YRuO_6, showing the only magnetic Ru ions.

The magnetic properties of the double perovskite Sr_2YRuO_6 are investigated using Monte Carlo simulations. The calculations are performed to simulate the Hamiltonian given in Eq. (1), considering the cyclic boundary conditions. For each spin configuration, we perform 10^5 Monte Carlo steps eliminating the first 10^4 generated configurations. While skimming all the system sites, single-flip attempts are made, and they either are accepted or rejected according to the Metropolis algorithm. In fact, the average of each parameter has been obtained for each Monte Carlo simulation, when averaging over several initial conditions, under the well-known Jackknife method.[29] For every iteration, the following parameters are calculated.

The internal energy per site

$$E = \frac{\langle H_S \rangle}{N_T}, \quad (2)$$

where N_T is the total number of atoms consisting the unit cell.

The magnetization of the system

$$M = \left\langle \sum_i S_i / N_T \right\rangle. \quad (3)$$

The susceptibility χ is given by

$$\chi = \frac{\langle M^2 \rangle - \langle M \rangle^2}{K_B T}, \quad (4)$$

where K_B is the Boltzmann constant fixed at its unit value ($K_B = 1$), and T is the absolute temperature. In this study, we will limit to the results of a fixed system size $N_T = 5 \times 5 \times 5$, using the free boundary conditions.

3. Results and discussion

3.1. The ground state phase diagrams

In order to study the ground state phase diagrams of the ruthenate compound Sr_2YRuO_6, we illustrate the corresponding phase diagrams in Figs. 3–5. The provided phase diagrams are obtained from the Hamiltonian of Eq. (1) by replacing the

spin values and comparing different energies. In the absence of any temperature fluctuations, we calculate the energy corresponding to each configuration and take the minimum one.

Figure 3 presents the ground state phase diagram in the plane (H, Δ) for $J_{\parallel} = 1$ and $J_{\perp} = -1$. The all possible four phases $+3/2$, $+1/2$, $-1/2$, and $-3/2$ are present in this figure. For $H > 0$, when $\Delta > 0$, the phase $+3/2$ is stable, while for $\Delta < 0$, the phase $+1/2$ is the stable one. For $H < 0$, when $\Delta > 0$, the phase $-3/2$ is stable, while for $\Delta < 0$, the phase $-1/2$ is the stable one. From this figure, a perfect symmetry with respect to the external magnetic field $H = 0$ appears. In particular, the specific point $(H = 0, \Delta = -2)$ corresponds to the coexistence of all the phases of $+3/2$, $+1/2$, $-1/2$, and $-3/2$. On the other hand, for $\Delta < -2$, when varying the external magnetic field, the all possible phases appear in this figure. While for $\Delta > -2$, taking positive values, the only possible stable phases are $+3/2$ and $-3/2$, this is due to the competition between the different physical parameters.

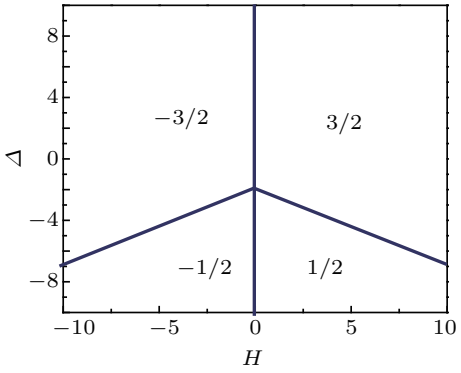


Fig. 3. Ground state phase diagram in the plane (H, Δ) for $J_{\parallel} = 1$ and $J_{\perp} = -1$.

To inspect the effect of the exchange coupling interactions, we illustrate in Fig. 4 the corresponding ground state phase diagram in the plane $(H, J_{\parallel})$ for $J_{\perp} = 1$ and $\Delta = -3$. The four possible phases are found in this figure. As shown in Fig. 3, a perfect symmetry is also present in this figure. The specific point $(H = 0, J_{\parallel} = 6.8)$ corresponds to the coexistence of the all possible phases. In particular, for $J_{\parallel}$ taking positive values, when varying the external magnetic field, we can find the existence of the all possible phases. While for $J_{\parallel}$ taking negative values, the only possible stable phases are $+1/2$ and $-1/2$, this is due to the antiferromagnetic behavior of the system. Such results have been confirmed experimentally in Refs. [30]–[32]. From Fig. 4, it is seen that for $J_{\parallel} < 6.6$, the all possible configurations are found to be stable, such results can be explained by the competition between the anisotropic effect of $J_{\parallel}$ and the external magnetic field.

Figures 5(a) and 5(b) show the effect of the competition between the crystal field and the exchange coupling $J_{\parallel}$ and $J_{\perp}$, respectively. From Fig. 5(a), the four stable phases are present in the plane $(J_{\parallel}, \Delta)$ for the values of $H = 0$ and $J_{\perp} = 1$. It is found that for $\Delta < -1$ and $J_{\parallel} < 10$, the stable phases are $\pm 1/2$. While for $J_{\parallel} > 10$ and $\Delta > -1$, the stable phases are $\pm 3/2$. These phases are separated by a linear curve with negative slope in the plane $(J_{\parallel}, \Delta)$. In particular, for $J_{\parallel} = 1$, the transition between the phases $\pm 1/2$ and $\pm 3/2$ is located at $\Delta = -1.86$.

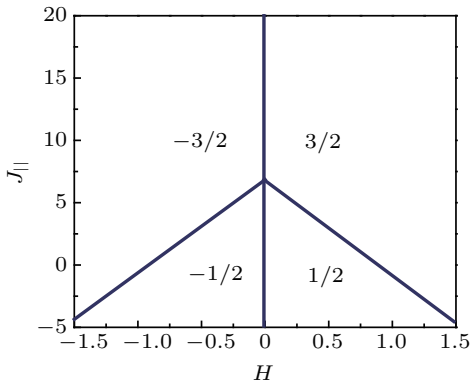


Fig. 4. Ground state phase diagram in the plane $(H, J_{\parallel})$ for $J_{\perp} = 1$ and $\Delta = -3$.

Figure 5(b), plotted in the plane $(J_{\perp}, \Delta)$, exhibits the same behavior with the same phases of $\pm 1/2$ and $\pm 3/2$. For a fixed value of $\Delta = -1$ and fixed exchange coupling $J_{\parallel} = -6$, for example, we find the stable phases to be $\pm 3/2$ in Fig. 5. Whereas for the same value of crystal field $\Delta = -1$ and fixed exchange coupling $J_{\perp} = -6$, we find that the stable phases are $\pm 1/2$. In particular, for $J_{\perp} = 1$, the transition between the phases $\pm 1/2$ and $\pm 3/2$ is located at $\Delta = -2.44$.

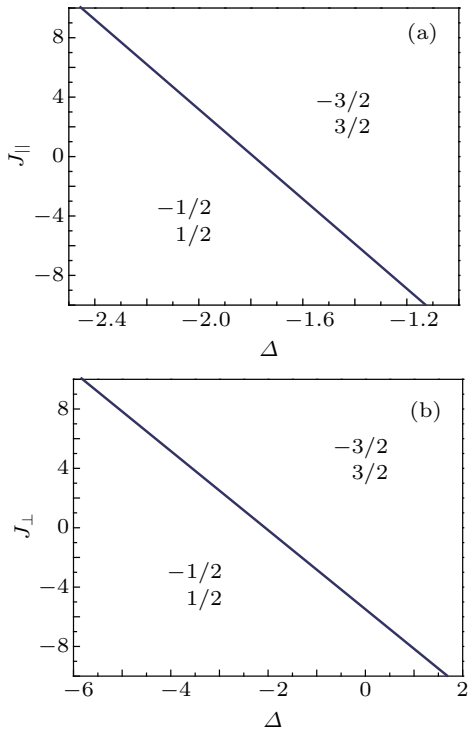


Fig. 5. Ground state phase diagram (a) in the plane $(J_{\parallel}, \Delta)$ for $H = 0$ and $J_{\perp} = 1$, (b) $(J_{\perp}, \Delta)$ for $H = 0$ and $J_{\parallel} = 1$.

3.2. Monte Carlo simulations

In order to show the behavior of both the magnetization and susceptibility of the double perovskite Sr_2YRuO_6 as a function of the temperature, we plot in Fig. 6 the obtained results for $\Delta = 15$, $J_{\parallel} = 0.025$, $J_{\perp} = -0.025$ in the absence of any external magnetic field ($H = 0$). This figure shows that for low temperatures, the saturation magnetization of the Ru^{5+} ion reaches 1.5, this is in good agreement with the obtained ground state phase diagram, see Fig. 5. The susceptibility as a function of the temperature manifests a peak around the critical temperature of $T_N = 31$ K, which is in good agreement with the experimental value.[1]

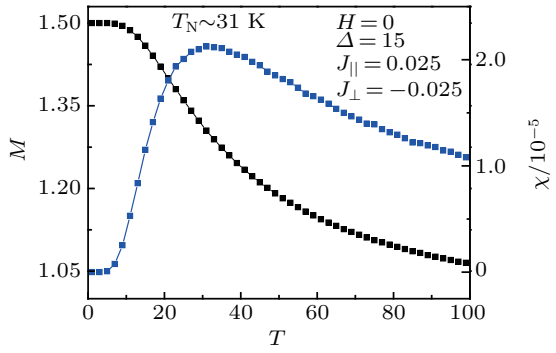


Fig. 6. Profiles of the magnetization and the susceptibility as a function of the temperature for $\Delta = 15$, $H = 0$, $J_{\parallel} = 0.025$, and $J_{\perp} = -0.025$.

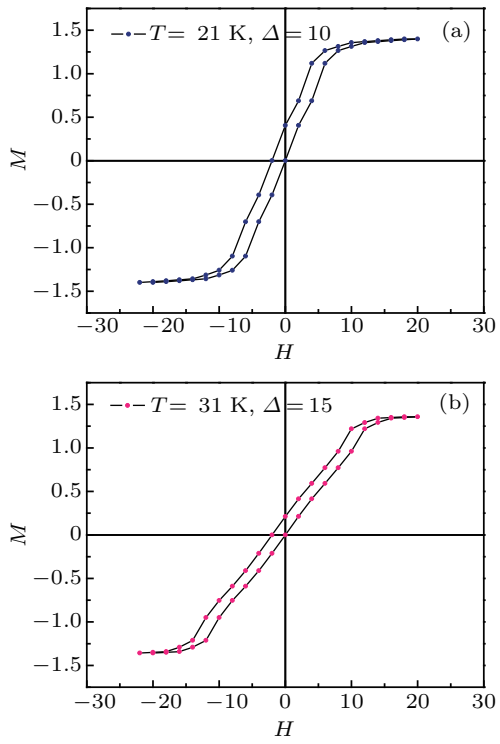


Fig. 7. The hysteresis loops of the Sr_2YRuO_6 compound as a function of the external magnetic field: (a) for $\Delta = 10$, $J_{\parallel} = 0.025$, $J_{\perp} = -0.025$, and $T = 21$ K; (b) for $\Delta = 15$, $J_{\parallel} = 0.025$, $J_{\perp} = -0.025$, and $T = 31$ K.

To complete this study, we provide in Fig. 7 the hysteresis loops of the Sr_2YRuO_6 compound as a function of the external magnetic field. In fact, we vary the different physical parameters in order to outline the effect as well as the competition between these parameters. For the case of Fig. 7(a), plotted for $\Delta = 10$, $J_{\parallel} = 0.025$, $J_{\perp} = -0.025$, and the fixed temperature $T = 21$ K, the saturation is reached at $H = 10$. In Fig. 7(b), illustrated for of $\Delta = 15$, $J_{\parallel} = 0.025$, $J_{\perp} = -0.025$, and the fixed temperature $T = 31$ K, the magnetization saturation is found at $H = 15$. This behavior is caused by the competition between the negative value of the exchange coupling $J_{\perp} = -0.025$ and the increasing of both temperature and crystal field. In fact, the magnetization saturation is reached when increasing or decreasing the external magnetic field, see Figs. 7(a) and 7(b). But the saturation magnetization depends not only on the temperature but also on the fixed value of the crystal field. It is worth to note that the obtained hysteresis cycles in Figs. 7(a) and 7(b) are asymmetric regarding the $H = 0$ axis. Such result is confirmed by experimental studies, see for example Refs. [30]–[32]. This phenomenon is due to the exchange bias effect produced by the antiferromagnetic interactions between the magnetic atoms of the compound Sr_2YRuO_6.

4. Conclusion

We have studied the magnetic properties of the double perovskite Sr_2YRuO_6 using Monte Carlo simulations. We presented and discussed the ground state phase diagrams at $T = 0$ K. We showed the effect of the competition between the crystal field and the exchange coupling $J_{\parallel}$ and $J_{\perp}$. The four possible phases are found to be stable in the plane $(J_{\parallel}, \Delta)$ for $H = 0$ and $J_{\perp} = 1$. Also we found that for $\Delta < -1$ and $J_{\parallel} < 10$, the only stable phases are $\pm 1/2$. While for $J_{\parallel} > 10$ and $\Delta > -1$, the stable phases are $\pm 3/2$. These phases are separated by a linear curve with negative slope in the plane $(J_{\parallel}, \Delta)$. The hysteresis loops of the Sr_2YRuO_6 compound as a function of the external magnetic field were presented and discussed. For $\Delta = 10$, $J_{\parallel} = 0.025$, $J_{\perp} = -0.025$, and the fixed temperature $T = 21$ K, the saturation is reached at $H = 10$. The delayed magnetization saturation is caused by the competition between the negative value of the exchange coupling and the increasing effect of both temperature and crystal field. We have also obtained the Néel temperature of Sr_2YRuO_6 ($T_N \approx 31$ K). The obtained results in this work are in good agreement with the earlier experimental results.[1]

References

[1] Singh R and Tomy C 2008 *Phys. Rev. B* **78** 024432
[2] Donohue P C and McCann E L 1977 *Mater. Res. Bull.* **12** 519
[3] Kuz'min E V, Ovchinnikov S G and Singh D J 2003 *J. Exp. Theor. Phys.* **96** 1124
[4] Dow J D and Harshman D R 2003 *Braz. J.* **33** 681
[5] Blackstead H A, Dow J D, Harshman D R, Yelon W B, Chen M X, Wu M K, Chen D Y, Chien F Z and Pulling D B 2001 *Phys. Rev. B* **63** 214412

[6] Harshman D R, Kossler W J, Greer A J, Stronach C E, Koster E, Hitti B, Wu M K, Chen D Y, Chien F Z, Blackstead H A and Dow J D 2000 *Physica B* **289** 360
[7] Harshman D R, Kossler W J, Greer A J, Noakes D R, Stronach C E, Koster E, Wu M K, Chien F Z, Franck J P, Dow J D and Isaac I 2003 *Phys. Rev. B* **67** 054509
[8] Demarco M, Blackstead H A, Dow J D, Wu M K, Chen D Y, Chien F Z, Haka M, Toorongian S and Fridmann J 2000 *Phys. Rev. B* **62** 301
[9] Rao S M, Srivastava J K, Wu M K, Mok B H, Chen C L, Ling M C, Liu H L, Chen Y Y and Ho J C 2011 *J. Supercond. Nov. Magn.* **24** 1249
[10] Rao S M, Wu M K, Srivastava J K, Mok B H, Yen N Y, Lin H Y, Tang H Y, Ling M C and Liu H L 2006 *Cryst. Res. Technol.* **41** 859
[11] Bernardo P L, Ghivelder L, Amorim H S, Neumeier J J and García S 2015 *New J. Phys.* **17** 103007
[12] Galstyan E, Xue Y Y, Iliev M N, Sun Y and Chu C W 2007 *Phys. Rev. B* **76** 014501
[13] Serrate D, De Teresa J M and Ibarra M R 2007 *J. Phys.: Condens. Matter* **19** 023201
[14] Mtougui S, Khalladi R, Ziti S, Labrim H and Bahmad L 2018 *Superlattices Microstruct.* **123** 111
[15] Mtougui S, Khalladi R, El Mekkaoui N, El Housni I, Idrissi S, Bahmad L, Ziti S and Labrim H 2018 *Comput. Condens. Matter* **17** e00329
[16] Mtougui S, Khalladi R, El Mekkaoui N, El Housni I, Idrissi S, Ziti S, Labrim H and Bahmad L 2018 *Comput. Condens. Matter* **17** e00331
[17] Idrissi S, Khalladi R, Ziti S, El Mekkaoui N, Mtougui S, Labrim H, El Housni I and Bahmad L 2019 *Physica B* **562** 116
[18] Idrissi S, Bahmad L, Khalladi R, El Housni I, El Mekkaoui N, Mtougui S, Labrim H and Ziti S 2019 *Chin. J. Phys.* **60** 549
[19] Idrissi S, Labrim H, Ziti S, Khalladi R, El Mekkaoui N, El Housni I, Mtougui S and Bahmad L 2019 *J. Electron. Mater.* **48** 3579
[20] El Housni I, Labrim H, El Mekkaoui N, Idrissi S, Khalladi R, Mtougui S, Ziti S and Bahmad L 2019 *Spin* **09** 1950002
[21] Idrissi S, Khalladi R, Mtougui S, Ziti S, Labrim H, El Housni I, El Mekkaoui N and Bahmad L 2019 *Physica A* **523** 714
[22] Idrissi S, Ziti S, Labrim H, Khalladi R, Mtougui S, El Mekkaoui N, El Housni I and Bahmad L 2019 *Physica A* **527** 121406
[23] Khalladi R, Labrim H, Idrissi S, Mtougui S, El Housni I, Ziti S, El Mekkaoui N and Bahmad L 2019 *Solid State Commun.* **290** 42
[24] Momma K and Izumi F 2011 *J. Appl. Crystallogr.* **44** 1272
[25] Aguirre M H, Logvinovich D, Bocher L, Robert R, Ebbinghaus S G and Weidenkaff A 2009 *Acta Mater.* **57** 108
[26] Naji S, Benyoussef A, El Kenz A, Ez-Zahraouy H and Loulidi M 2012 *Phys. A Stat. Mech. Its Appl.* **391** 3885
[27] Labrim H, Jabar A, Belhaj A, Ziti S, Bahmad L, Laânab L and Benyoussef A 2015 *J. Alloys Compd.* **641** 37
[28] Masrour R, Bahmad L and Benyoussef A 2012 *J. Magn. Magn. Mater.* **324** 3991
[29] Miller R G 1974 *Biometrika* **61** 1
[30] Folcke E, Le Breton J M, Lefebvre W, Bran J, Lardé R, Golkar F and Shield J E 2013 *J. Appl. Phys.* **113** 183903
[31] Chen J Y, Xu H J and Coey J M D 2014 *Appl. Phys. Lett.* **104** 152405
[32] Lestrer Clinton barnsley 2012 *Exchange Bias in Manganese Alloys with Mixed Magnetic Behaviour* (PhD Dissertation) (Brisbane: Griffith University)